Kinetic Monte Carlo simulation of self-organized growth of PbSe/PbEuTe quantum dot multilayers

M. Mixa,[1] V. Holý,[1] G. Springholz,[2] and G. Bauer[2]
[1]*Department of Condensed Matter Physics, Charles University, 12116 Prague, Czech Republic*
[2]*Institut für Halbleiterphysik, Johannes Kepler Universität, A-4040 Linz, Austria*
(Received 28 April 2009; revised manuscript received 25 June 2009; published 28 July 2009)

The heteroepitaxial growth in self-assembled quantum dot multilayers is investigated using kinetic Monte Carlo simulations and a quantitative comparison with experiment is included. We study the self-organization effect in the PbSe/PbEuTe(111) semiconductor system. For this purpose we developed an efficient kinetic Monte Carlo model enabling us to simulate multilayers consisting of tens of periods with hundreds of three-dimensional islands. We corroborate that the lateral and vertical-dot correlations are caused mainly by the strain field induced by buried dots. A progressive self-ordering from period to period in a growing multilayer is clearly illustrated. We also reproduced all three experimentally observed dot arrangements in the PbSe/PbEuTe(111) superlattices inclusive of two abrupt transitions between them. Moreover, we achieved a good quantitative agreement with the experimentally measured dependence of lateral-dot distance on spacer-layer thickness. The advantages and shortcomings of our model are analyzed in detail.

DOI: 10.1103/PhysRevB.80.045325 PACS number(s): 64.75.Yz, 68.55.A−, 68.65.Cd, 81.16.Rf

I. INTRODUCTION

Quantum dots (QDs) as a class of semiconductor nanostructures are recently intensively studied due to their unique electrical and optical properties, and great potential for device applications. The spontaneous formation of three-dimensional (3D) quantum dots (islands) in the Stranski-Krastanow growth mode of strained heteroepitaxial layers is a promising candidate for QD fabrication.[1–3] For technological purposes a high-density, uniform-size distribution and regular arrangement of defect-free dots are required. The spatial dot density can be increased significantly by growing QD multilayers, generating a 3D superlattice of buried islands. A sophisticated technique for achieving a laterally and vertically well-ordered QD multilayer is the use of the *self-organization effect*, where the buried QDs influence positions and sizes of the dots in the subsequent layers.[2,4]

The strain field induced by a lattice mismatch between the materials of QDs and of the spacer layer is mostly responsible for the self-organization effect. The elastic deformation of the spacer due to the mismatch of its lattice with respect to the QD lattice produces energetically more favorable areas on the spacer surface, where the island nucleation is enhanced.[5–7] This is a typical self-organization mechanism where also the elastic anisotropy of deposited materials and the surface orientation play a significant role. They fundamentally affect the lateral and vertical correlations in a growing QD superlattice. A theoretical analysis has been given by Holý *et al.*[8]

An interesting example of a self-assembled system are PbSe/PbEuTe(111) multilayers[9] with the Eu content ranging from 5% to 10%. The PbSe dots form well-faceted trilateral pyramids with {100} side facets.[10] Depending on the PbEuTe spacer-layer thickness, three different dot arrangements are observed.[11] A vertical-dot alignment is found in multilayers with a spacer period thinner than approximately 37 nm. For spacer thicknesses ranging from 37 to 56 nm the dots form a fcc-like 3D trigonal lattice (an *ABCABC* stacking) with a tunable lattice constant. In both these cases a pronounced hexagonal lateral ordering of the QD positions is observed.[11,12] When the spacer thickness exceeds approximately 56 nm, the islands grow uncorrelated both in lateral and vertical directions, i.e., such multilayers are completely disordered.

Much effort has been devoted to the development of numerical simulations of self-assembled growth in nanostructures. The simulations considerably facilitate finding the optimal growth conditions and also improve the understanding of relevant growth processes. The kinetic Monte Carlo (KMC) method has been successfully used for atomistic simulations of epitaxial growth in numerous papers.[13–16] Additionally, the growth in two-dimensional (2D) islands on prepatterned substrates[16,17] or periodically strained surfaces[18,19] has been studied. The effect of different growth parameters on the final surface morphology was investigated in details by Meixner *et al.*[20] and many others. Pan *et al.*[21] studied the QD ordering on GaAs substrates with different surface orientation and confirmed a strong influence of elastic anisotropy on the resulting QD patterns. Zhu *et al.*[22] recently proposed a fast multiscale KMC model designed for simulation of 3D self-assembled QD layers. Russo and Smereka[23] proposed another 3D KMC model for strained epitaxial growth simulation using a ball and spring-type model for incorporation of the strain effects. Vertical correlations of stacked QDs in dependence on spacer-layer thickness were also successfully examined using the KMC method.[24,25]

On the other hand, as far as we know, nobody has reported KMC simulations of self-organized *multilayer* growth corresponding to a particular semiconductor system, moreover with a good quantitative agreement with experiment. In this paper we present KMC simulations modeling the molecular-beam epitaxial growth in PbSe/PbEuTe(111) multilayers. We show that our KMC model can reproduce their self-ordering properties described above. An enhanced dot arrangement from period to period in the simulated multilay-

ers is clearly demonstrated together with the obtained dependence of lateral-dot distance on spacer thickness which is in a good quantitative agreement with experiment.

II. THEORY

This work is focused on the investigation of the self-organized nucleation of QDs in PbSe/PbEuTe(111) multilayers. We do not deal with the formation of a wetting layer (WL), i.e., with the 2D to 3D growth transition, nor with the detailed shape of the growing dots. Our simulation includes the movement of free-standing adatoms on the WL surface, so that the simulation process in each period starts just at the moment when the wetting-layer formation is finished (in the sense that it has achieved its critical thickness) and the QDs start to grow.

A. Strain field calculation

It is well known from thermodynamic reasons that the QDs nucleate predominantly in minima of chemical potential and that the surface diffusion of adatoms is governed by the gradient of the chemical potential.[26] In the commonly used continuum approach, the chemical potential μ of an adatom can be written as[27,28]

$$\mu(s) = \mu_0 + w(s)V_0 + \gamma\kappa(s)V_0, \tag{1}$$

where s denotes a point along the surface, μ_0 is a reference value of the chemical potential, w is the volume density of elastic energy, γ is the surface tension, κ is the surface curvature, and V_0 is the atomic volume. In the continuum approach the third term is related (via the surface curvature) to the number of free chemical bonds of a free-standing adatom. Since the formed WL is assumed to be atomically flat, we consider this term to be constant for all equilibrium sites on the WL. From this assumption we get a relation for the difference in μ in two neighboring equilibrium sites (on an atomically flat WL): $\Delta\mu = \Delta w V_0$.

The elastic energy density is given by the relation

$$w(s) = \frac{1}{2} C_{ijkl}\epsilon_{ij}(s)\epsilon_{kl}(s), \tag{2}$$

where C_{ijkl} are the elastic constants and ϵ_{ij} is the strain tensor. Due to the linearity of the elasticity theory for small deformations, the strain tensor (in a given point s on the WL surface) can be written as a sum of pseudomorphic deformation $\epsilon_{ij}^{\mathrm{pseu}}$ of the WL, and the individual strain contributions $\epsilon_{ij}^{\mathrm{QD}}$ caused by all QDs buried in previous periods under the WL

$$\epsilon_{ij} = \epsilon_{ij}^{\mathrm{pseu}} + \sum_{\text{buried QDs}} \epsilon_{ij}^{\mathrm{QD}}, \quad i,j = 1,2,3. \tag{3}$$

The elastic strain $\epsilon_{ij}^{\mathrm{QD}}$ from a buried QD can be calculated by a semianalytical method[8,29,30] based on the solution of the equilibrium equation of continuum. The method is applicable to an arbitrary surface orientation and it also considers the elastic anisotropy of crystalline materials. Nevertheless, it uses an important assumption that the surface of the dot-covering spacer must be flat. We assume it is well satisfied for buried dots, however, this requirement excludes this method for the calculation of a strain induced by uncovered dots on the sample surface.

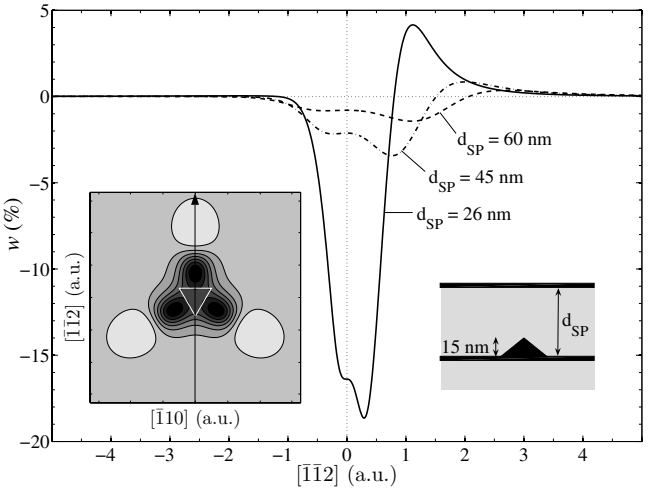

FIG. 1. Line profiles of relative elastic-energy density w calculated on the PbSe(111) WL surface for three different PbEuTe spacer thicknesses d_{SP}. The strain field is produced by a buried dot of a height of 15 nm (see the right inset scheme). The left inset shows the surface distribution of w for d_{SP}=45 nm. The dark color corresponds to an energy minimum, the arrow denotes the profiles' direction, and the white triangle denotes the buried-dot base.

In a general case during the deposition, when some dots are already grown on the topmost WL, their strain contributions should also be incorporated in the summation in Eq. (3). Nevertheless, at the initial phase of the nucleation of QDs, the strain field is well described by Eq. (3) and that is the essence of our work. Moreover, as we have just mentioned, the applied strain-calculation method cannot be used for uncovered dots. For these reasons, the strain field from growing dots is omitted in Eq. (3).

As an example, the line profiles of relative elastic-energy density calculated for three different PbEuTe spacer thicknesses d_{SP} are demonstrated in Fig. 1. The profiles are taken along the lateral $[\bar{1}\bar{1}2]$ direction on the (111) WL surface. The deformation is caused by a PbSe pyramidal dot with {100} facets and a height of 15 nm covered by a given spacer. The left inset in Fig. 1 shows a lateral distribution of w corresponding to d_{SP}=45 nm. Three separated energy minima around the centrum appear due to the elastic anisotropy of the PbEuTe material and the (111) surface orientation. They predetermine the nucleation positions on the WL. Their depth and separation distance strongly depend on the spacer thickness d_{SP}. In the strain calculations we use the following values of the elastic constants: $(c_{11}=12.37,\ c_{12}=1.93,\ c_{44}=1.59)\times 10^{11}$ dyn/cm^2 for PbSe,[31] and $(c_{11}=10.53,\ c_{12}=0.70,\ c_{44}=1.32)\times 10^{11}$ dyn/cm^2 for PbTe.[32]

B. Model description

We apply an event-based KMC scheme[33,34] to investigate the nucleation process and the self-organized QD growth. The basic processes included in an adapted solid-on-solid

model[13] are the deposition of adatoms onto the surface and their subsequent surface diffusion. By an *adatom* we understand one "PbSe molecule" that always moves on the simulation grid as a whole. The adatom desorption is omitted from the model since it is negligible under the usual growth conditions. The surface diffusion of adatoms is modeled as a sequence of nearest-neighbor hops on a square lattice. Since the adatom migration is a thermally activated process, the hopping rate k of an adatom onto a nearest-neighbor site is given by the Arrhenius-type formula

$$k_{i\to f} = k_0 \exp(-E_{i\to f}/k_B T), \tag{4}$$

where $k_0 = 2k_B T/h \sim 10^{13}$ s^{-1} is a characteristic vibrational frequency, T is the substrate temperature, k_B is Boltzmann's constant, and h is Planck's constant. $E_{i\to f}$ denotes the energy barrier which an adatom must overcome at a hop from the initial site i to the final site f. Motivated by Eq. (1) and the comment below it, we express $E_{i\to f}$ as a sum of two terms: a substrate term E_S and a strain-field contribution induced by buried dots

$$E_{i\to f} = E_S + K(w_f - w_i)a_{cell}^3. \tag{5}$$

E_S corresponds to a position-independent hopping barrier on unstrained surface. w_i and w_f are the elastic energy densities at the sites i and f calculated from Eq. (2), where ϵ_{ij} is calculated according to Eq. (3) comprehensive of all dots buried under the just growing layer. a_{cell} is the linear size of a simulation cell. The coefficient $K>0$ is a free input parameter of the model. It enables the study of the strain-field influence on the self-organization effect. Strictly speaking, instead of w_f the value of w in the point where the hopping barrier has its maximum (between the sites i and f) should be applied. Because we evaluate the strain field only in the equilibrium sites, we replace the "middle value" by a linear interpolation between the values w_i and w_f and the interpolation coefficient is effectively incorporated in K.

Let us note the main simplifications of the described KMC model that is not strictly atomistic. We have already mentioned that neither the WL formation nor the shape of growing dots is atomistically simulated. The dot shape is taken *ad hoc* from the experiment[10] and thus the dots are modeled as trilateral pyramids with {100} side facets. When an adatom joins an existing dot, the dot size is increased but its shape and the coordinates of the center of the dot base remain unchanged. No structural changes in the dots during the overgrowth process are considered as well. The main advantage of this approximation is that the simulations are substantially faster, so a larger area and more multilayer periods can be simulated, which is more important for the self-organization effect study. The second significant simplification is the use of a square grid although the PbSe(111) surface does not possess the square symmetry. To ensure a corresponding scale, it is required the same number of equilibrium sites in a unit area as it would be on the real PbSe(111) surface. From this condition the a_{cell} is given as $a_{cell} = (\sqrt[4]{3}/2)a_{\mathrm{PbSe}}$, where a_{PbSe} is the PbSe lattice constant.

On the other hand, the existence of a critical nucleus,[35] consisting of N_c adatoms, is included in the model. We consider a nonzero probability of an adatom escape from a dot smaller than the critical nucleus. All dots of size equal to or larger than the critical nucleus are taken as absolutely stable, i.e., the escape probability is set to zero for them. The escape rate k^e for a nucleus consisting of just two adatoms is calculated as

$$k^e(2) = k_0 \exp[-(E_S + E_B)/k_B T], \tag{6}$$

where E_B is the binding energy between two adatoms at neighboring sites. The typical value of this energy for semiconductor materials is about $0.2 \sim 0.3$ eV (Refs. 20 and 36) and we do not include any strain-field influence on it. The rate $k^e(N)$ of an adatom escape from a nucleus of size N $(2<N<N_c)$ is calculated simply by linear interpolation between the values $k^e(2)$ and $k^e(N_c)=0$. This approximation is motivated by the knowledge that a nucleus becomes more and more stable due to its growth.

Also the nuclei are represented by trilateral pyramids during their growth. If two (or more) free adatoms meet at neighboring sites, they join together and create a new dot (nucleus) in such a way that its triangular base is marked out on the simulation grid. Each simulation cell of the grid is always in one of three possible states: unoccupied, occupied by an adatom, or occupied by a dot. The edge length of the triangular base corresponding to a dot containing N adatoms is calculated from the expression: $\sqrt[3]{12\sqrt{2}Na_{cell}^3}$ (the dot volume is considered to be Na_{cell}^3). When an adatom splits off from a nucleus, the nucleus base is reduced and the split-off adatom is placed at a randomly selected site whose distance from the base margin is equal to two cells. (Sites at the distance of one cell directly touch the base and an adatom placed there would immediately join the nucleus again.)

The described part of the model is very important since it allows a total decay of any undercritical nucleus. Let us remark that in all cited references to other KMC growth simulations,[13–25,33,34,36] the concept of critical nucleus is included implicitly by using a bond-counting model, where the hopping probability depends on the number of occupied neighboring sites.

Beside the possible events in our KMC model (the deposition, a free-standing adatom hop, and an adatom escape from a nucleus), the dot-coalescence effect is also taken into account. If two or more dots intersect on the simulation grid due to their growth, they are replaced by a new dot created between them. The volume of the new dot is a sum of the original dots' volumes. Let us mention for completeness that the growth conditions are constant for all periods and *no* prepatterned substrate is used, as well as in experiment.

Finally, let us comment on the thermodynamic equilibrium in our simulations. The simulated system, developing according to the introduced model, successively moves toward a limit state where all deposited adatoms are comprised in totally stable (i.e., supercritical) dots. This state is completely static and is achievable always if the total number of all deposited adatoms is greater than the critical nucleus size N_c. Since the simulations stop as soon as all adatoms are deposited, some unstable nuclei and free adatoms can remain on the surface as well. We assume that such final state of a simulation corresponds well to the situation in experiment after the QDs' growth if no extra annealing is applied. In this

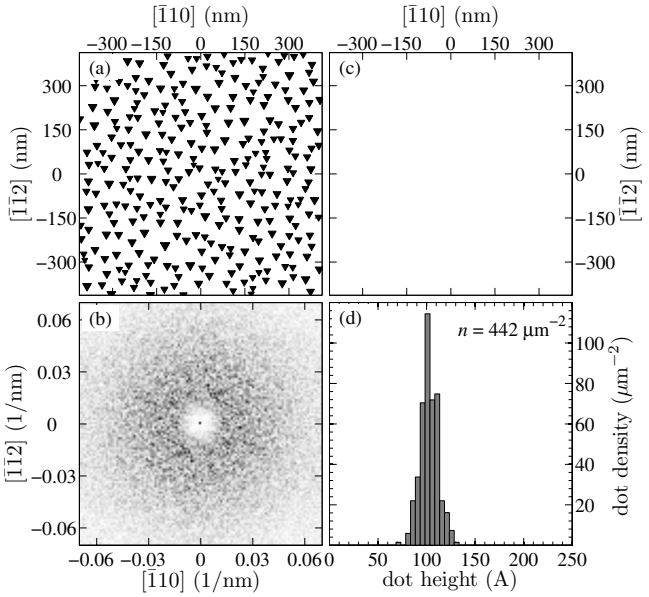

FIG. 2. Analysis of the first multilayer period: (a) dot positions and sizes (a top view), (b) 2D FFT power spectrum of the surface morphology, (c) the cross-correlation function (it is blank here), and (d) the dot-height histogram.

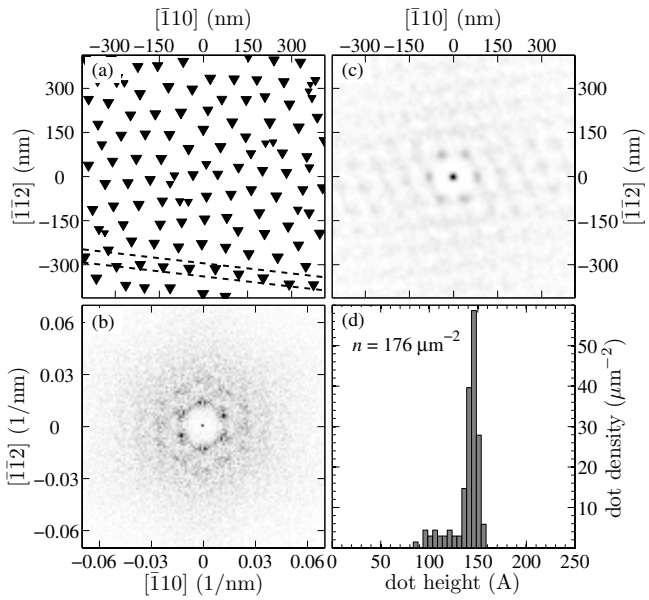

FIG. 3. Analysis of the 20th period of a multilayer simulated with a thin spacer of $d_{SP}=26$ nm. (a) Dot positions and sizes (a top view), (b) 2D FFT power spectrum of the surface morphology, (c) the cross-correlation function of the 19th and 20th dot-layer surface morphology, and (d) the dot-height histogram. The two dashed lines in (a) mark out the location of the vertical cross section through this multilayer displayed in Fig. 6(a).

sense we do not explicitly deal with the detailed balance condition[37] since we do not require achievement of the (real) thermodynamic equilibrium specified by the Boltzmann distribution. The essential fact is that our description of the adatom surface diffusion, given by Eqs. (4) and (5), prefers the occurrence (and thus the nucleation) of adatoms at sites with lower energy (chemical potential), which corresponds to the reality.

III. RESULTS

All presented simulations were carried out on a simulation grid of 2048×2048 cells (an area of 0.7 μm^2) under typical experimental conditions: substrate temperature $T=370$ °C, deposition flux F of PbSe molecules of 0.12 ML/s, and total PbSe coverage of 5 ML. The remaining model parameters were determined from simulations of the first (unstrained) layer as follows. The dot-height histogram from the first layer is compared with experimental data to achieve the best agreement. From tens of various combinations of the parameters' values we found the following optimum values: $E_S=0.93$ eV, $E_B=0.2$ eV, and the part of the total PbSe coverage (5 ML) used just for the formation of dots of 1.2 ML. The optimum value of the critical nucleus size was determined from the simulations of the growth in the whole multilayer and it was estimated to $N_c=100$ adatoms (PbSe molecules). This value corresponds to a trilateral pyramid with an edge of about 4.6 nm, which is in good agreement with Mayer's work,[38] where the size was estimated from energy calculations using the continuum elasticity as about 5.0 nm. The coefficient K remains a free parameter and its influence on the results is analyzed below. Let us mention in advance that its optimum value was found to be $K=7$.

In Fig. 2 the result of the simulation of the first layer is displayed. The grown dots are completely uncorrelated since there is no strain from buried dots, which would affect the deposited atoms, and so all sites in the first layer are energetically equivalent. No correlation is also proved at the fast Fourier transform (FFT) power spectrum [Fig. 2(b)], where no satellite peaks occur. The dot density $n=442$ μm^{-2} is typical for the experimental conditions mentioned above. Absence of a previous dot layer also caused the blank cross-correlation function [Fig. 2(c)].

Using the KMC model described in Sec. II we can mimic all three kinds of the PbSe/PbEuTe multilayers' arrangement. It is shown in Figs. 3–5, where the topmost (20th) dot layers are displayed. They belong to three multilayers simulated with different spacer thickness of 26, 45, and 60 nm, respectively.

For $d_{SP}=26$ nm we obtain a vertically aligned multilayer as is clearly visible from the cross-correlation function [Fig. 3(c)] showing a pronounced maximum at the coordinate-system midpoint. That implies a vertical reproduction of the surface morphology in subsequent layers. The dot density (in the 20th period) strongly decreases to 176 μm^{-2} and the dot-height histogram [Fig. 3(d)] becomes significantly narrower. Due to the self-organization effect the dots form a disordered 2D hexagonal array [Fig. 3(a)] which is more obvious in Fig. 3(b) depicting the FFT power spectrum where one can recognize six satellite peaks.

The *ABCABC* stacking achieved in the simulation with $d_{SP}=45$ nm is pictured in Fig. 4. The cross-correlation function has three main maxima close to the coordinate center and a minimum at the center, which corresponds to the *ABCABC* stacking. The dot-height histogram again becomes narrower with respect to the first-layer one. Dot density de-

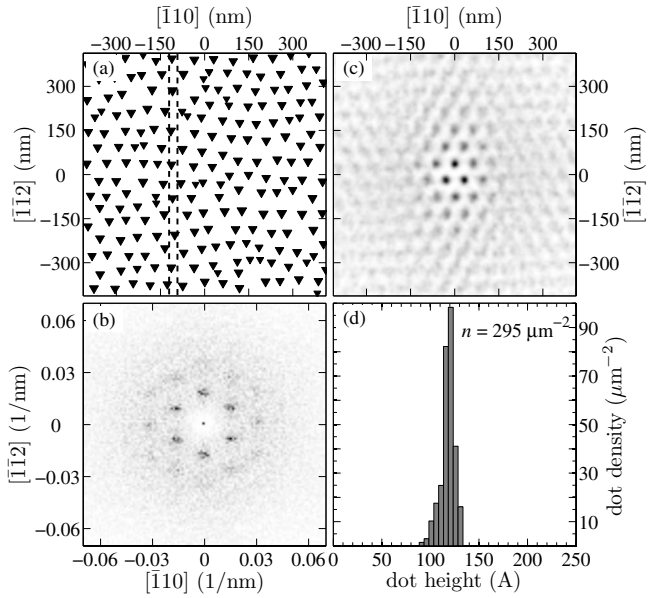

FIG. 4. Analysis of the 20th period of a multilayer simulated with an intermediate spacer of d_{SP}=45 nm. [(a), (b), (c), and (d)] Description is the same as in Fig. 3. The two dashed lines in (a) mark out the location of the vertical cross section through this multilayer displayed in Fig. 6(b).

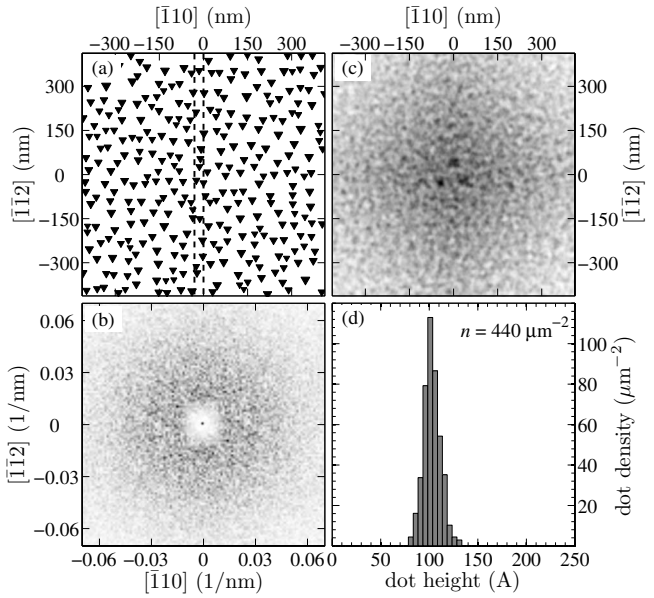

FIG. 5. Analysis of the 20th period of a multilayer simulated with a thick spacer of d_{SP}=60 nm. [(a), (b), (c), and (d)] Description is the same as in Fig. 3. The two dashed lines in (a) mark out the location of the vertical cross section through this multilayer displayed in Fig. 6(c).

creases to 295 μm^{-2} and the dots laterally self-organize themselves into a more shapely hexagonal structure than in the previous (vertical) case. It is demonstrated by sharper satellite peaks in the FFT power spectrum [Fig. 4(b)].

A simulation carried out with d_{SP}=60 nm produced an uncorrelated multilayer displayed in Fig. 5. The dots grown in the last layer are completely disordered like in the first one (Fig. 2). The dot density of 440 μm^{-2} remains nearly identical with the first layer and also the FFT power spectrum does not change significantly. It does not contain any peaks which would reveal a lateral correlation in the dot positions. In Fig. 5(c) of cross-correlation function one can recognize three indistinct maxima indicating a negligible residual correlation in the vertical direction.

The dashed lines in Figs. 3(a), 4(a), and 5(a) mark out locations of the vertical cross sections through the grown multilayers. The cross sections are depicted in Fig. 6. For the multilayer simulated with d_{SP}=26 nm, the cross section is taken along a direction slightly deflected from the [1̄10] direction and its width is 60 nm. For the multilayers with d_{SP}=45 nm and 60 nm, the cross sections are identically taken along the [1̄1̄2] direction and their width is 35 nm. The color of the QD-representing triangles indicates their relative position in the cross-sectional band orthogonally to the cross section. Let us rather note that the impression of a higher dot density of the multilayer in Fig. 6(a) is deceptive and caused only due to the different orientation and width of the cross section. The cross sections graphically show the progressive evolution of the QD-superlattice self-organization. The superlattice with the thick spacer [Fig. 6(c)] remains apparently disordered in all periods. Figure 6(b) vice versa proves the *ABCABC* stacking, well visible mainly in the last five periods, of the superlattice with the intermediate spacer. The replication angle of the dot positions of 39° to the surface normal is in perfect agreement with the identical experimental value.[11] Well pronounced vertical ordering of the superlattice simulated with the thin spacer is clearly visible in Fig. 6(a).

The progressive self-organization evolution of those analyzed multilayers is quantitatively characterized in Fig. 7 which shows the dependence of dot density n, lateral-dot distance L, and lateral correlation length L^{corr} versus the period number. The dot density in the ordered multilayers (d_{SP}=26 and 45 nm) exhibits a strong decrease immediately in the first superimposed periods [see Fig. 7(a)]. Then its value starts to be more or less constant from the 10th period approximately. The third curve, belonging to the uncorrelated multilayer, exhibits only statistical fluctuations around a fixed value, as expected by virtue of no ordering in that multilayer. L and L^{corr} were determined from the separation of FFT satellite peaks and their broadness, respectively, for the ordered multilayers. While L only slightly increases with increasing period number [see Fig. 7(b)], L^{corr} conversely shows a strong enhancement [see Fig. 7(c)] corresponding to a larger and larger evenly ordered area of QDs. The L^{corr} dependence also shows that the lateral-dot arrangement is superior and improves more steeply in the *ABCABC* stacked multilayer than in the vertically aligned one, which accords with experiment.

Figure 8 compares the experimentally measured dependence of L on d_{SP}, where L is the mean lateral distance between dots in the topmost layer, with the one obtained from our KMC simulations. The two vertical dashed lines in the graph denote two critical spacer thicknesses that correspond to the observed transitions between the different kinds of superlattice arrangement. In experiment, the transition from a vertical alignment (region I, *thin spacers*) to an

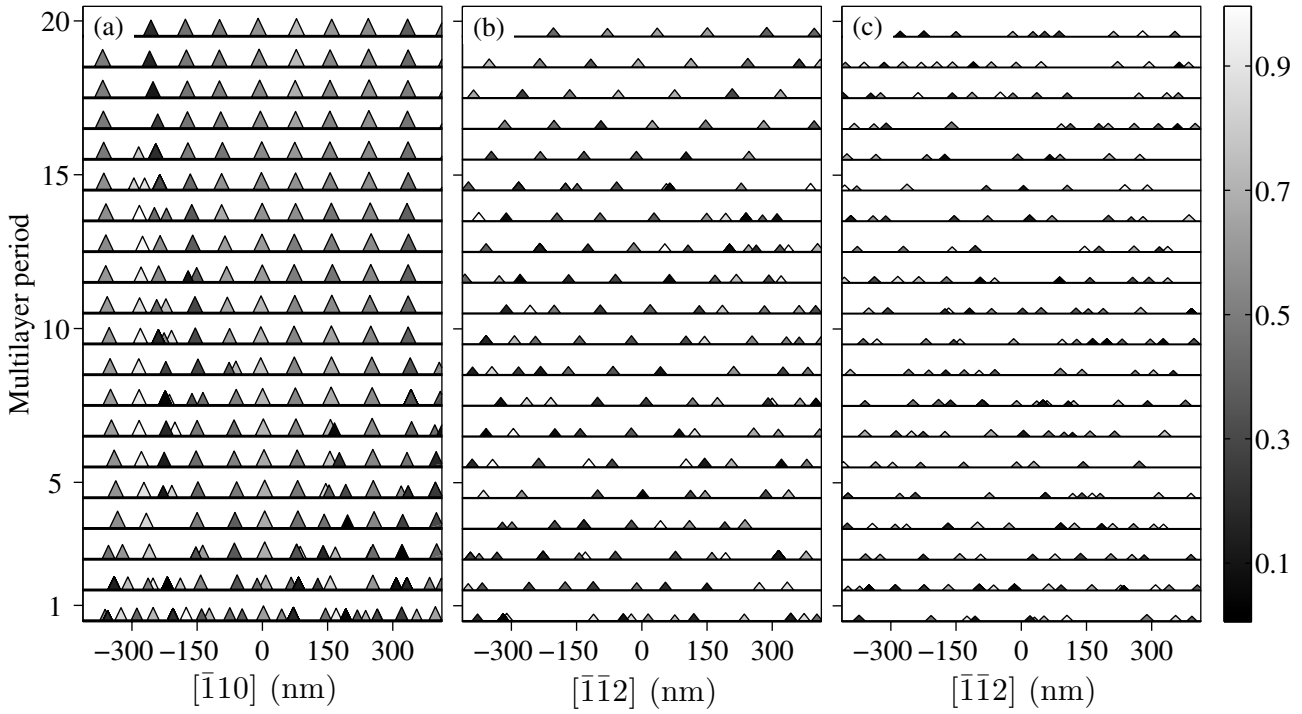

FIG. 6. Vertical cross sections through multilayers consisting of 20 periods simulated with different spacer thicknesses d_{SP}: (a) 26 nm; (b) 45 nm; and (c) 60 nm. The lateral orientation and location of the cross-section bands are denoted in Figs. 3(a), 4(a), and 5(a), respectively, by two dashed lines. The gray level of the QD-representing triangles relatively indicates their complementary lateral coordinate in the related cross-section band.

ABCABC stacking (region II, *intermediate spacers*) arises at d_{SP} of around 37 nm and the second one from the *ABCABC* stacking to the uncorrelated mode (region III, *thick spacers*) at d_{SP} of around 56 nm. All KMC simulations were carried out with the optimum set of input parameters and a stack of 20 periods was always simulated. The growth conditions of the experimental samples were very similar: in region I: $T=360$ °C, $F=0.12$ ML/s, and 50 superlattice periods;[12] in regions II and III: $T=360$ °C, $F=0.08$ ML/s, and 30 periods.[11] For the disordered multilayers (region III), L is calculated from n via $L=1/\sqrt{n\cdot\sin 60°}$ which would correspond to a dot separation in a perfectly hexagonally ordered layer just with the dot density n.

From Fig. 8 we can see that the position of the second transition and the abruptness of both transitions are successfully reproduced by the simulations. Further, the increasing linear dependence of L on d_{SP} obtained for the intermediate spacers agrees well with experimental measurements (see Fig. 8, region II). A small difference in L is visible in the uncorrelated region III. That is due to the slightly different growth conditions in the experiment and the simulations, leading to little diverse dot densities and hence to diverse L in this region. A systematic discrepancy is vice versa obvious at the thin spacers where all experimental values of L are by about 10-nm larger, although the character of the dependence is very similar (see Fig. 8, region I). Moreover, the first structural transition occurs at a thinner spacer of about 33 nm, instead of 37 nm. Both these discrepancies are discussed in Sec. IV.

At the end of this section, let us turn the attention to the coefficient K. This prefactor in Eq. (5) has, due to the exponential character of Eq. (4), a substantial influence on the adatoms' kinetics and thus on the self-organization process. If we set $K=1$, then all multilayers with a spacer thicker than 24 nm end up completely disordered. From this reason we have to enhance the K value to obtain results accordant with the experiment. An increase in K does not alter a pattern of w but only magnifies its "gradient" with respect to the substrate energy barrier E_S in Eq. (5). In other words, it does not directly affect the form of a resulting QD arrangement, but mainly its quality. Table I presents such results. It contains some values of n, L, and L^{corr} describing a lateral ordering of QDs obtained from simulations where only K and d_{SP} varied. (20-period multilayers were simulated again and the data are from the topmost period.)

For the thin-spacer multilayers ($d_{SP}=26$ nm) one can see that the values of n, L, and L^{corr} do not vary significantly, i.e., statistically identical superlattices are practically formed for all $K=5,7,10$. For $d_{SP}=45$ nm a divergence is already appreciable. While the values of L are more or less equivalent again, n and L^{corr} change with K distinctly (see the middle rows of Table I). $K=5$ causes a weaker ordering illustrated by a higher n and reduced L^{corr}. The higher dot density but equal L (determined from FFT) imply that the QDs oftentimes grow (at $K=5$) even out of the preferred energy minima separated by L. On the contrary, $K=10$ yields a larger L^{corr}, i.e., a more regular hexagonal lateral ordering. However, $K=10$ also causes a partial arrangement of the multilayer simulated with the thick spacer of 60 nm (see the last row in Table I) and that is in contradiction with experiment. All around, the results show that the position of the second critical spacer in Fig. 8 can be controlled (in the

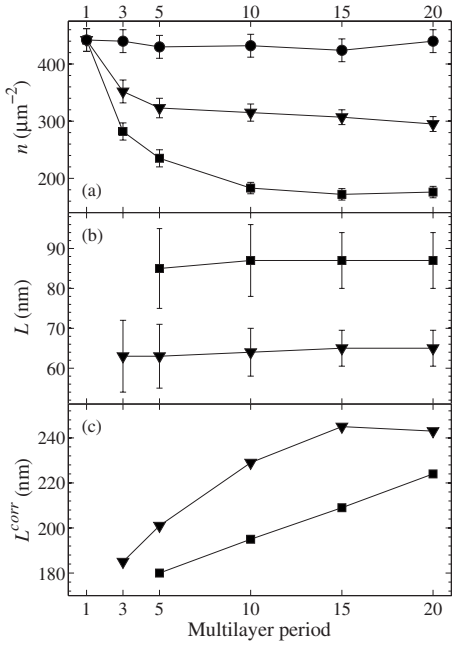

FIG. 7. Evolution of: (a) dot density n; (b) lateral-dot distance L; and (c) lateral correlation length L^{corr} as a function of multilayer-period number. Square symbols belong to the multilayer simulated with d_{SP}=26 nm; triangles to d_{SP}=45 nm, and circles to d_{SP} =60 nm. L and L^{corr} were determined from the separation of FFT satellite peaks and their broadness, respectively. The relative error of L^{corr} can be only roughly estimated, due to the simulation-area limited size, to be about 20%-30% (the lower error holds for higher periods).

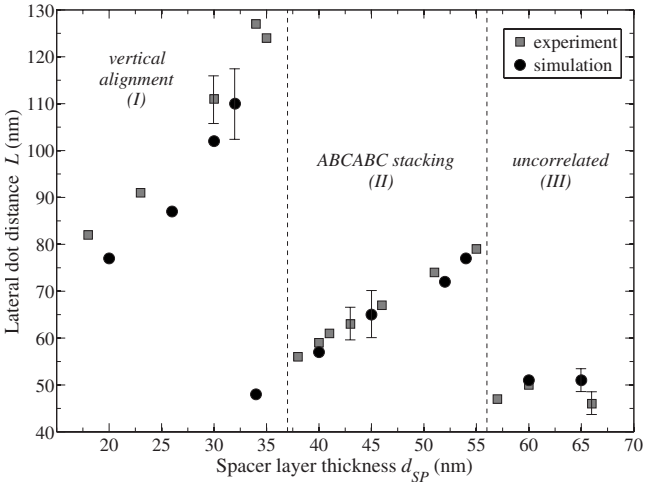

FIG. 8. Comparison of experimental and simulation results. The lateral-dot distance is plotted versus spacer-layer thickness. The two vertical dashed lines denote the experimentally found positions of two critical spacers corresponding to observed transitions between different QD arrangements. The error bars at some data points represent typical errors.

simulations of course) just by the coefficient K. From the listed arguments, we found the most suitable value of K to be 7 (within the framework of the presented model and the simulated semiconductor system). To K we turn back also in the discussion (Sec. IV B).

IV. DISCUSSION

A. Comparison with experiment

The presented KMC simulations confirmed that the self-organization effect in the PbSe/PbEuTe(111) multilayers is induced mainly by the strain field caused by buried dots since no other mechanism is taken into account in our KMC model. It seems the main shortcoming of the used model is the omission of the deformation produced by growing dots at the free surface. Nevertheless, positions of the QD nuclei at the *initial* phase of deposition are governed just by the strain field from *buried* QDs (if no defects, steps, etc. are considered). So the related distribution of elastic-energy minima on the WL surface also exclusively predetermines the final lateral-dot distances. This statement is well corroborated by the comparison of the simulation and experimental results in Fig. 8. At the later deposition phases the strain field from growing dots may surely play an important role, however, the comparison documents a fundamental role of the buried QDs. The influence of growing dots will naturally be more relevant if the growing QDs are large, which is the case of the thin-spacers region. This could explain the systematic shift of the simulation results in region I in Fig. 8. But there are some other effects such as overgrowth changes or uneven surface of the spacer layer (more probable at thin spacers) that could contribute to the observed difference between the simulations and experiment as well.

For completeness, let us comment on the differences between simulation and experimental growth conditions of the multilayers compared in Fig. 8, particularly the unequal number of superlattice periods. Figure 8 compares the mean lateral-dot distance L at the topmost period and Fig. 7(b)

TABLE I. Dependence of dot-arrangement parameters (dot density n, lateral-dot distance L, and lateral correlation length L^{corr}) at the topmost layer on the coefficient K, for three different spacer thicknesses d_{SP}.

K	n (μm^{-2})	L (nm)	L^{corr} (nm)
	d_{SP}=26 nm		
5	159	89	216
7	176	87	224
10	178	88	209
	d_{SP}=45 nm		
5	384	63	192
7	295	65	243
10	274	66	287
	d_{SP}=60 nm		
5	430	*disordered*	
7	440	*disordered*	
10	335	81	221

shows that L does not significantly vary at higher period numbers, so the unequal number of periods is irrelevant here. (Of course, this need not be true for the lateral correlation length L^{corr}, etc.) Despite the slightly different growth conditions, the simulations revealed a nearly identical L vs d_{SP} dependence for the intermediate spacers and the same trend of this dependence at thin spacers. It confirms again that L in ordered multilayers is strongly predetermined through the buried-dots strain field. (The *slight* difference in the growth conditions is crucial here of course). The small difference in L determined from n at the uncorrelated multilayers has already been explained just by the different growth conditions.

The discrepancy in the position of the first critical spacer (see Fig. 8) is probably given by the simple dot-coalescence model. We believe that the transition between the vertical alignment and the *ABCABC* stacking proceeds in the following way. In a multilayer with a spacer thickness comparable to the first critical spacer, three distinctly separated energy minima (like in the left inset in Fig. 1) are induced by each buried dot (with a proper height) on the next WL surface. Subsequently, three new QDs nucleate *separately* in these minima. Depending on the minima spacing and the deposition coverage the three dots coalesce together or not. If they coalesce, they form a large QD above the buried dot, i.e., the vertical alignment is produced. Vice versa, if they do not coalesce, the vertical alignment does not occur and the strain field caused by them at the subsequent layer will favor separated islands again. Hence the *ABCABC* stacking will occur. The dot-coalescence process and its conditions in reality are of course more complex than the ones used in our model. Furthermore, the longer L measured in experiment at thin spacers implies larger QDs on the surface, ergo more suitable conditions for their coalescence again. Therefore we observe the first transition at a little thinner spacer in the simulations.

B. The *K* coefficient

The most disputable matter of the simulations is the coefficient K. Its optimum value ($K=7$) was determined so that the best agreement with experiment was achieved. The K coefficient can be understood as a correction factor comprising all shortcomings of the model. For example, if the critical nucleus concept is removed from the model (i.e., all pairs of encountered adatoms create stable QDs), K must be increased to about 40 to achieve any accordant results. So the introduction of a critical nucleus existence enabled to reduce K up to 7. With increasing N_c (size of the critical nucleus in the model) the required value of K progressively decreases. However, there is a saturation effect since the simulations performed with $N_c=1000$ no longer statistically differ from those performed with $N_c=100$ but these differ from those simulated with $N_c=50$. These results also document the indispensability of the critical nucleus existence for a correct simulation of the self-organization process in the Stranski-Krastanow growth mode.

Surprisingly, K (within the range from 5 to 10) does not considerably influence the arrangement of multilayers having thin spacers (see the data in Table I for $d_{SP}=26$ nm). It is due to the aforementioned fact that K can just alter the amplitude of a strain-field modulation but not the shape of its surface distribution. It only intensifies the nucleation of QDs in local strain-energy minima. The strain-energy minima caused by QDs covered by a thin spacer are significantly deeper than the ones in an intermediate-spacer case (see Fig. 1). Therefore, at thin spacers, K need not be too high to ensure a good vertical alignment. And since a higher K does not adjust the shape of w on the WL surface, the lateral ordering is not affected much by K varying within the mentioned range. It holds generally that K can improve particularly the vertical correlations and less the lateral ones. We infer this is the reason why the lateral correlation length L^{corr} still comes out shorter than in experiment in both ordered regions I and II.

There is also one other issue related with K that should be discussed. It is concerned with limitations of the continuum theory if one deals with the surface diffusion of individual adatoms. The commonly used Eq. (1) contains the atomic volume V_0 which is not a clearly and exactly specified quantity. The term $w(s)V_0$ in Eq. (1) should express a work necessary to produce a coherent match between a surface and an element of mass V_0 (that is going to be strained for this purpose).[27] However, a coherent match or an elastic deformation is well defined for an element of *continuum* but not for a single adatom. Therefore, we are on a continuum approach applicability limit and the uncertainty of the V_0 specification is effectively incorporated into the K coefficient in Eq. (5). On the other hand, the well-reproduced L vs d_{SP} dependence inclusive of the two abrupt changes (Fig. 8), which is closely related to a surface distribution of w, indicates that the adatom hopping barrier modeled by Eq. (5) may have a good foundation. An alternative option how to incorporate the strain effects is using of a ball- and spring-type model as Russo and Smereka[23] used.

We suppose that K includes all simplifications and neglects made in the model. Namely: missing strain field from growing dots, uncertainty of the V_0 determination, strain influence on some other material parameters e.g., E_S, E_B, and N_c; square lattice use, modeling of QD nuclei as 3D pyramids, and linear dependence of the adatom escape rate $k^e(N)$ on the nucleus size N. The important point is that the same value of K yields a reasonably good correspondence with the experimental data for *all* simulated spacer thicknesses. Therefore it seems that the parameter K could plausibly substitute all the effects listed above.

C. Comparison with other models

The most significant difference of the presented KMC model from others is the noncounting of adatom's neighbors (bonds). The other KMC models used for QDs epitaxial growth studies[13–25,33,34,36] are miscellaneous variations in a bond-counting model. In our model, the conventional bond-counting approach and detailed atomistic monitoring of a structure of the growing (2D or 3D) islands are substituted by the critical nucleus concept and a fixed (but arbitrary adjustable) shape of the simulated QDs. It prohibits us to study a shape evolution of the nuclei or stable dots, an adatom migration around island boundaries, etc. However, the model

is designed for a simulation of self-organized QD *multilayer* growth. The grown QDs are 3D but their shape is not intricately treated in detail.[22,23] This reveals the essential advantage of the introduced model: to simulate realistic 3D superlattices consisting of tens of periods with hundreds of 3D QDs in each period. The possibility, characteristic for the KMC method, to investigate different growth conditions is retained of course.

Despite a relative simplicity, the model yields results in good quantitative agreement with experiment concerning the observed vertical and lateral correlations at a concrete semiconductor system PbSe/PbEuTe(111). The results also perfectly agree with the general theoretical predictions of Shchukin *et al.*[6] and KMC simulations done by Meixner and Schöll[25] relating to a vertical correlation-anticorrelation transition in dependence on spacer layer thickness. Kunert and Schöll[39] stress out the importance of finite volume of QDs and inclusion of elastic interactions in an array of buried QDs to reproduce an abrupt correlation-anticorrelation transition in QD stacks. Both these features are just incorporated in our model and such an abrupt transition is really observed. The QDs self-organized themselves from a completely disordered first layer, in accordance with the experiment, and the uniformity of island size and spacing progressively enhanced from period to period as Tersoff *et al.*[5] formerly introduced.

V. CONCLUSION

In this paper, we have introduced a KMC model designed for efficient realistic simulations of heteroepitaxial growth of QD multilayers. The model differs from the others by the noncounting of adatom's bonds and a preset 3D shape of the growing dots. It explicitly includes a critical nucleus existence whose presence has proved to be fundamental. The simulation results focused on the lateral- and vertical-dot correlations in the PbSe/PbEuTe(111) multilayers clearly verified their source in the strain field from buried dots. All three types of vertical-dot correlations known for the studied system were successfully reproduced as well as a reasonably good quantitative comparison with the experimentally measured dependence of lateral-dot distance on spacer layer thickness. The presented model has been adapted to the PbSe/PbEuTe(111) system, however, it is totally general and it can be used for an arbitrary semiconductor (crystalline) system with any surface orientation or can be easily modified, e.g., for prepatterned substrates.

ACKNOWLEDGMENTS

The authors are grateful to R. Sýkora (Charles University in Prague) for valuable discussions. This work is a part of the research program (Grant No. MSM 0021620834) that is financed by the Ministry of Education of the Czech Republic; the work has been also supported by the EC SANDiE European Network of Excellence and by the Project No. KAN400100652 of the Grant Agency of the Academy of Sciences of Czech Republic.

[1] D. Bimberg, M. Grundmann, and N. N. Ledentsov, *Quantum Dot Heterostructures* (Wiley, New York, 1999).
[2] J. Stangl, V. Holý, and G. Bauer, Rev. Mod. Phys. **76**, 725 (2004).
[3] V. A. Shchukin and D. Bimberg, Rev. Mod. Phys. **71**, 1125 (1999).
[4] G. Springholz and V. Holý, in *Lateral Alignment of Epitaxial Quantum Dots*, edited by O. G. Schmidt (Springer-Verlag, Berlin, 2006), pp. 247–303.
[5] J. Tersoff, C. Teichert, and M. G. Lagally, Phys. Rev. Lett. **76**, 1675 (1996).
[6] V. A. Shchukin, D. Bimberg, V. G. Malyshkin, and N. N. Ledentsov, Phys. Rev. B **57**, 12262 (1998).
[7] R. Marchetti, F. Montalenti, L. Miglio, G. Capellini, M. De Seta, and F. Evangelisti, Appl. Phys. Lett. **87**, 261919 (2005).
[8] V. Holý, G. Springholz, M. Pinczolits, and G. Bauer, Phys. Rev. Lett. **83**, 356 (1999).
[9] G. Springholz, V. Holý, M. Pinczolits, and G. Bauer, Science **282**, 734 (1998).
[10] M. Pinczolits, G. Springholz, and G. Bauer, Appl. Phys. Lett. **73**, 250 (1998).
[11] G. Springholz, M. Pinczolits, P. Mayer, V. Holý, G. Bauer, H. H. Kang, and L. Salamanca-Riba, Phys. Rev. Lett. **84**, 4669 (2000).
[12] A. Raab, R. T. Lechner, and G. Springholz, Appl. Phys. Lett. **80**, 1273 (2002).
[13] P. Šmilauer and D. D. Vvedensky, Phys. Rev. B **52**, 14263 (1995).
[14] C. Ratsch, P. Šmilauer, D. D. Vvedensky, and A. Zangwill, J. Phys. I **6**, 575 (1996).
[15] K. E. Khor and S. Das Sarma, Phys. Rev. B **62**, 16657 (2000).
[16] L. Nurminen, A. Kuronen, and K. Kaski, Phys. Rev. B **63**, 035407 (2000).
[17] W. Guo, R. S. Guico, J. M. Xu, and R. Beresford, J. Vac. Sci. Technol. B **25**, 1072 (2007).
[18] M. I. Larsson, R. F. Sabiryanov, K. Cho, and B. M. Clemens, J. Appl. Phys. **94**, 3470 (2003).
[19] C. Zhao, Y. H. Chen, C. X. Cui, B. Xu, J. Sun, W. Lei, L. K. Lu, and Z. G. Wang, J. Chem. Phys. **123**, 094708 (2005).
[20] M. Meixner, R. Kunert, and E. Schöll, Phys. Rev. B **67**, 195301 (2003).
[21] E. Pan, R. Zhu, and P. W. Chung, J. Appl. Phys. **100**, 013527 (2006).
[22] R. Zhu, E. Pan, and P. W. Chung, Phys. Rev. B **75**, 205339 (2007).
[23] G. Russo and P. Smereka, J. Comput. Phys. **214**, 809 (2006).
[24] C. S. Lee, B. Kahng, and A. L. Barabási, Appl. Phys. Lett. **78**, 984 (2001).
[25] M. Meixner and E. Schöll, Phys. Rev. B **67**, 121202(R) (2003).
[26] W. W. Mullins, J. Appl. Phys. **28**, 333 (1957).
[27] R. J. Asaro and W. A. Tiller, Metall. Trans. **3**, 1789 (1972).
[28] H. Gao, J. Mech. Phys. Solids **42**, 741 (1994).
[29] V. Holý, T. U. Schülli, R. T. Lechner, G. Springholz, and G.

Bauer, J. Alloys Compd. **401**, 4 (2005).
[30] T. Roch, V. Holý, A. Hesse, J. Stangl, T. Fromherz, G. Bauer, T. H. Metzger, and S. Ferrer, Phys. Rev. B **65**, 245324 (2002).
[31] G. Lippmann, P. Kästner, and W. Wanninger, Phys. Status Solidi A **6**, K159 (1971).
[32] A. J. Miller, G. A. Saunders, and Y. K. Yogurtcu, J. Phys. C **14**, 1569 (1981).
[33] E. Schöll and S. Bose, Solid-State Electron. **42**, 1587 (1998).
[34] M. Meixner, E. Schöll, V. A. Shchukin, and D. Bimberg, Phys. Rev. Lett. **87**, 236101 (2001).
[35] J. Tersoff and F. K. LeGoues, Phys. Rev. Lett. **72**, 3570 (1994).
[36] P. Šmilauer and D. D. Vvedensky, Phys. Rev. B **48**, 17603 (1993).
[37] M. E. J. Newman and G. T. Barkema, *Monte Carlo Methods in Statistical Physics* (Clarendon, Oxford, 1999).
[38] P. Mayer, Diploma thesis, Institut für Halbleiterphysik, University of Linz, 2001.
[39] R. Kunert and E. Schöll, Appl. Phys. Lett. **89**, 153103 (2006).